Observation of silicon front surface topographs of an ultralarge-scale-integrated wafer by synchrotron x-ray plane wave

Yoshifumi Suzuki[a] and Yoshimitsu Tsukasaki
Faculty of Engineering, Kyushu Institute of Technology, Sensui-cho, Tobata-ku, Kitakyushu-shi 804-8550, Japan

Kentaro Kajiwara
Japan Synchrotron Research Institute, SPring-8, Mikazuki-cho, Hyogo 679-5198, Japan

Seiji Kawado
Rigaku Corporation, Akishima-shi, Tokyo 196-8666, Japan

Satoshi Iida
Faculty of Science, Toyama University, Toyama 930-8555, Japan

Yoshinori Chikaura
Faculty of Engineering, Kyushu Institute of Technology, Sensui-cho, Tobata-ku, Kitakyushu-shi 804-8550, Japan

(Received 28 June 2004; accepted 8 September 2004)

Surface roughness and undulation of unpatterned silicon wafers are serious issues for ultralarge-scale-integrated circuit devices, even after fine mechanochemical polishing. It has never been clarified whether the undulations exist only on the surface or also exist inside the bulk crystal. We produced grazing incident diffraction topographs at three x-ray photon energies, with penetration depths estimated to be 3.85 nm, 4.78 nm, and 1.28 μm. All the topographs contained striation. We also obtained clear total reflection images using synchrotron x-ray plane waves, which also showed striation patterns at penetration depths from 3.85 nm to 1.28 μm. These results indicate that the origin of the patterns is not at the surface but is inside the Si wafer. The origin of striation patterns, observed in the topographs, was found not to be due to mechanochemical polishing processes but to crystal growth. © *2004 American Institute of Physics*. [DOI: 10.1063/1.1812354]

I. INTRODUCTION

"Nanotopography" refers to the study of 10–100-nm surface undulations on lateral millimeter length scale unpatterned silicon wafers.[1] Nowadays, the isolation scheme is commonly used for the fabrication of Si-ultralarge-scale-integration (Si-ULSI) devices for dimensions as low as 0.2 μm. In the fabrication of Si-ULSI devices, surface roughness and undulation are serious issues, even after fine mechanochemical polishing. The surface of these devices can be mapped by the Nanomapper™ surface mapping system, which uses optical interferometry from phase shifts and is appropriate for 200- and 300-mm wafers. However, this system provides whole wafer topography measurements only of the surface of polished wafers.[2] X-ray topography and total reflection methods, on the other hand, allow characterization not only of the surface of a wafer, but also the interior of a bulk crystal, the depth dependence being dependent on the glancing angle. We have designed and constructed a high-resolution diffraction topography station, located at the medium-length (200 m) bending magnet beam line of the Biomedical Imaging Center, BL20, SPring-8.[3,4] Conventional standard reflection topography gives information about the crystal to a depth of an extinction distance, typically several microns. The particular point of going to critical angle grazing incidence is to reduce and control the penetration depth to the submicron range.

We present the topographic, asymmetry grazing incident diffraction (GID) geometry of 8-in. (20-cm) double-sided mechanochemical-polished silicon wafers around the critical angle ($\alpha_c \sim 0.07°$) using ~22.7 keV energy x-rays and the relatively higher density of nanotopography on surface features observed by Nanomapper™. GID measurements are capable of observing not only the wafer surface but also the interior of the bulk crystal. We present step-scanned x-ray topographs, with multiexposure and 5 arcsec step angle, showing so-called zebra patterns[5] and circular patterns. Patterns similar to the circlelike patterns are also observed in optical measurements. No microdefects are seen in the enlarged pictures. We also present total reflection topographs obtained at a glancing angle smaller than the critical angle. We discuss the origin of the striation patterns.

II. EXPERIMENT

Wafers were prepared from *p*-type (Boron-doped 1.581×10^{19}–1.753×10^{19} atoms/cm^3) 200-mm-diameter Czochralski silicon crystals with a [100] surface orientation and a resistivity range of 0.007 05–0.006 38 Ω cm. The crystals were sliced into wafers with a wire saw. The surfaces of the wafers were lapped with #1000-meshed powder and polished mechanically and chemically by the both-sided polish

[a]Electronic mail: ysuzuki@e-lab.kyutch.ac.jp

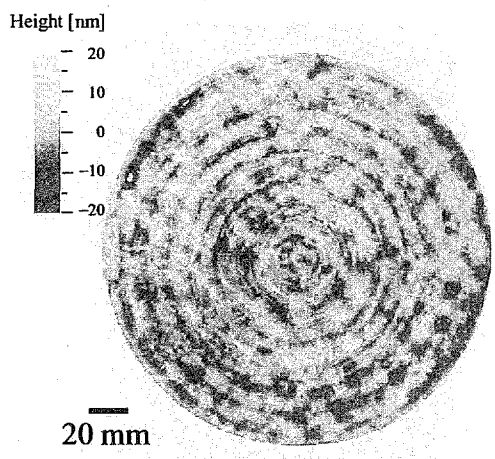

FIG. 1. Nanotopography map from Nanomapper™ optical measurement.

method. The sample thickness was 0.5 mm and the wafer included comparably higher density of nanotopography on surface features. Figure 1 shows a nanotopography map by Nanomapper™ optical measurements, revealing a wavy texture with a difference in height of angstrom order. However, the surface appears mirrorlike in conventional visible measurements.

Figure 2 shows a schematic diagram of the experimental arrangement for large-area x-ray diffraction topography measurements. A 300-mm-wide monochromatic x-ray beam, obtained from the bending magnet source 200 m away from the experimental hutch, was used to acquire topographs of large-diameter silicon wafer samples.[4,5] The samples were fixed without glue onto a flat plastic plate attached on a horizontal-axis precision tangential-bar-type goniometer.[5] In the experimental setting at BL20B2, the sample and topograph film cassette were set in experimental hutch 2 and the total reflection photograph cassette was set in hutch 3. GID geometry, 511 reflection, observations were performed. In the total reflection photograph experiments, the distance between sample and film was set at 9.09 m, so as to prevent a strong direct beam and hence obtain clear total reflection images. Images were obtained on x-ray Agfa D2 films and also on an imaging plate with a pixel size of 100×100 μm^2 read by an imaging-plate reader and then processed on a personal computer.

III. RESULTS AND DISCUSSION

We can easily estimate the glancing angle α_i by the equation $\tan 2\alpha_i = h/l$, where h is the distance between the direct beam and the total reflection beam point and l is the distance between the sample and the film cassette point ($\sim$9.09 m in Fig. 2). We can calculate the x-ray penetration depth ξ by Eq. (1) for wavelength λ, linear absorption coefficient μ, and critical angle α_c. The critical angle was estimated from the wavelength and the density of silicon.

$$\xi = \frac{\sqrt{2}\lambda}{4\pi\{(2\delta-\sin^2\alpha_i)+[(\sin^2\alpha_i-2\delta)^2+(2\beta)^2]^{1/2}\}^{1/2}}, \tag{1}$$

where $2\delta=\sin^2\alpha_c$ and $\beta=\mu\lambda/4\pi$.[6] This equation applies not only to crystals but to all solid and liquid states.

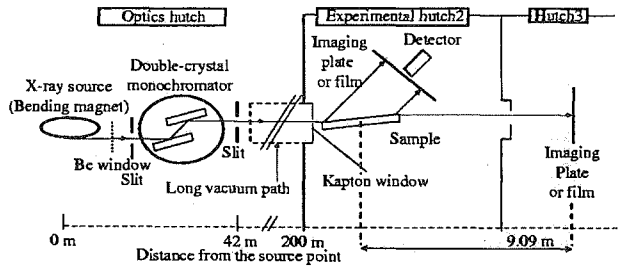

FIG. 2. Schematic diagram of experimental arrangement for large-area x-ray diffraction topography and total reflection.

TABLE I. Experimental parameters and penetration depths calculated by Eq. (1).

	E [keV]	λ [Å]	α_c [mrad]	α_i [mrad]	α_i/α_c	β	ξ [Å]
a	22.67	0.5470	1.367	1.650	1.207	2.934×10^{-9}	12880
b	22.72	0.5457	1.364	1.018	0.7458	2.906×10^{-9}	49
c	22.78	0.5443	1.361	0.7717	0.5671	2.877×10^{-9}	39

Experimental parameters and penetration depths calculated by Eq. (1) are given in Table I. The labeled *a*, *b*, and *c* represent the three different sets of conditions shown in Table I. The Eq. (1) and Table I indicate that the penetration depth varies from a few nanometers to a few micrometers, depending on the incident angle.

Before recording topographs and total reflection images, rocking-curve measurements were carried out over a 2×4 mm^2 area on the sample with a scintillation counter at a rotation rate ω at a fixed angle $2\theta_B$ (θ_B: Bragg angle). As a typical example, Fig. 3 shows the rocking curve for condition *c* in Table I. The full width at half maximum of the rocking curves for the conditions *a*, *b*, and *c* were 6.59, 6.85, and 5.54 arcsec, which are very similar in value.

We made 511 reflection, GID geometry observations for each of the conditions *a*, *b*, and *c* on 8-in. double-sided mechanochemical-polished silicon wafers around the critical angle ($\alpha_c\sim0.0780°$–$0.0784°$) using $\sim$22.78–22.67 keV x-rays, including observations of comparably higher density of nanotopography on surface features. Figures 4 and 5 show typical multiexposure step-scanned x-ray topographs with 5 arcsec step angle for the conditions *c* and *a*, respectively. Figure 4 was taken using an imaging plate and was enlarged in the **g** direction by computer in order to make the length scale the same for both the parallel and perpendicular directions. Figure 5 was taken using x-ray film without correction. We can observe the so-called zebra patterns[5] and circular

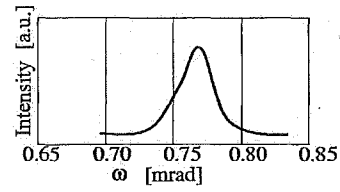

FIG. 3. Rocking curve at an x-ray energy of 22.78 keV for condition *c* in Table I.

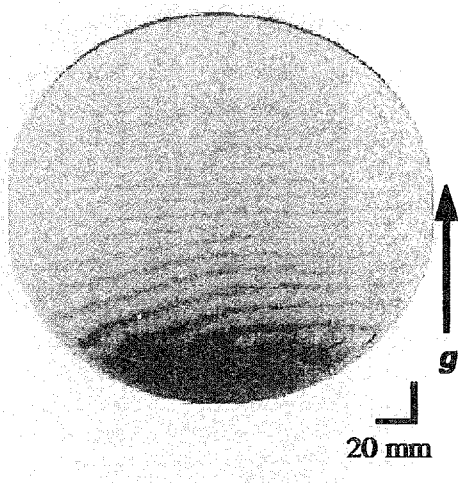

FIG. 4. Step-scanned 511 GID x-ray multiexposure topograph on an imaging plate. The raw data is condensed in the g direction and hence the image was enlarged in the **g** direction by computer in order to make the length scale the same in both the parallel and perpendicular directions.

patterns in these figures. The Bragg condition was satisfied only in one stripe area at each step angle, so a zebra pattern could only be obtained with multiexposures. They are equal inclination contours and provide a sensitive measure of wafer bending. The circular pattern is similar to the pattern observed in the optical measurement in Fig. 1. No microdefects are seen in Fig. 4, taken with an imaging plate, or in Fig. 5, where the higher-resolution x-ray film was used. We

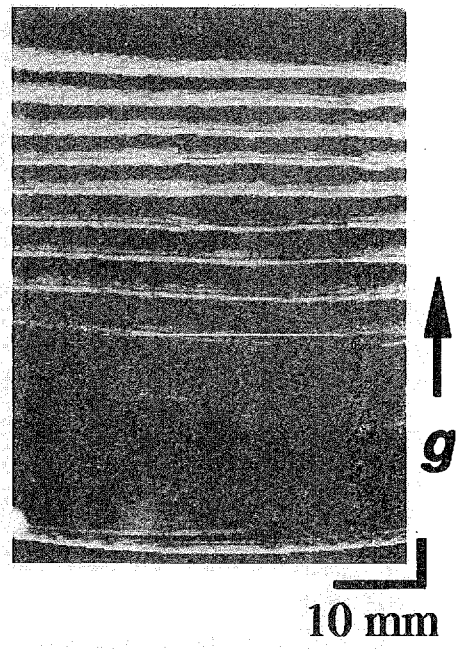

FIG. 5. Step-scanned 511 GID x-ray multiexposure topograph on an x-ray film. Although it is impossible to make a correction for shrinkage, it is possible to enlarge with a higher resolution than an imaging plate. A deformed circular pattern can be seen in this image.

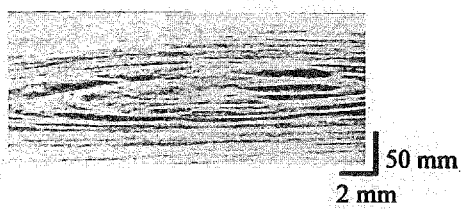

FIG. 6. Total reflection image for condition b using an x-ray film, showing deformed circular pattern.

observed striation patterns at all depths from 3.85 nm to 1.28 μm from the surface, showing that the striation patterns originate inside the bulk of the crystals.

Although GID measurements are capable of observing the vicinity of a wafer surface,[7] it is difficult to satisfy the Bragg condition on large areas of a bending wafer. It is easier to obtain a total reflection image than a GID measurement. For each of the conditions a, b, and c, we observed clear total reflection images. Figure 6 shows, as a typical example, a total reflection image for condition b (22.72 keV), in spite of a large shrinkage in the direction parallel to the x-ray beam. As with the diffraction topographs, the total reflection images were similar to the optical measurement in Fig. 1. We observed striation patterns at all depths from 3.85 nm to 1.28 μm from the surface, showing that the striation patterns originate inside the bulk of the crystals.

IV. CONCLUSIONS

We obtained GID topographs for x-ray penetration depths of 3.85 nm, 4.78 nm, and 1.28 μm, as well as the first clear total reflection images. All topographs showed striation patterns, including patterns at penetration depths from 3.85 nm to 1.28 μm. This indicates that the origin of the patterns is not at the surface but inside the wafer. This result provides valuable information for research into the growth of Si crystals.

ACKNOWLEDGMENTS

The authors are grateful to Komatsu Electronic Co. Ltd. for supplying the samples. This work was carried out according to the SPring-8 proposal number 2002A0272-ND3-np. Technical support from Dr. Y. Suzuki, Dr. K. Umetani, and Dr. K. Uesugi at SPring-8 is also appreciated.

[1]SEMI DRAFT Document 3089 (1999), p. 1.
[2]S. Xu, Electrochem. Solid-State Lett. **1**, 181 (1998).
[3]Y. Chikaura, S. Iida, S. Kawado, K. Mizuno, S. Kimura, J. Matsui, M. Umeno, T. Ozaki, T. Shimura, Y. Suzuki, K. Izumi, K. Kawasaki, K. Kajiwara, and T. Ishikawa, J. Phys. D **34**, A158 (2001).
[4]S. Kawado, S. Iida, and Y. Chikaura, SPring-8 Reseach Frontiers (1999/2000) 89.
[5]S. Kawado, S. Iida, S. Yamaguchi, S. Kimura, Y. Hirose, K. Kajiwara, Y. Chikaura, and M. Umeno, J. Synchrotron Radiat. **9**, 166 (2002).
[6]H. Dosch, Phys. Rev. B **35**, 2137 (1987).
[7]S. Kimura, J. Mizuki, J. Matsui, and T. Ishikawa, Appl. Phys. Lett. **60**, 2604 (1992).